A global climate model with strechable grid and nudging: I. simulation of tracer transport at continental scales

A. Idelkadi, P. LeVan and F. Hourdin *
Laboratoire de Météorogogie dynamique du CNRS, IPSL, Paris, France

Draft, 10th October 2005

Abstract

In the frame of climate change modeling, global atmospheric circulation models have been developed in the past decade which include a representation of large scale and turbulent transport of trace species. Here, the tracer component of the LMDZ general circulation model is presented and evaluated using the results of the European Tracer EXperiment (ETEX). For that purpose the model winds are nudged by operational analyzes from operational weather forecast centers and the global grid is refined over Europe. The model compares satisfactorily well with other dispersion models with some interesting specificities due to its global grid and interactive physical parameterizations. ETEX is used to assess the different model capabilities (nudging, zoom, transport scheme diffusivity, unplugged mode). The nudged and zoomed model is a powerful tool for validation of the tracer component but can also be used for assessment of physical parameterizations as discussed in a companion paper.

1. Introduction

Coupling between spatial variations of atmospheric constituents and atmospheric general circulation is important in the frame of global change studies. In order to study couplings between atmospheric trace constituents and global atmospheric circulation, a number of modeling efforts have been undertaken recently. First attempts were conducted with so-called chemistry transport models forced by observed or modeled winds. The "radiative forcing" deduced from these **off-line** computations was then introduced back in the climate models to estimate the impact on climate.

*Corresponding author, Laboratoire de Météorologie Dynamique, UPMC, Tour 45-55, 3eme étage, BP-99, Jussieu, 4 place Jussieu, 75 005 Paris, France, hourdin@lmd.jussieu.fr

More recently, people started to implement directly parameterizations of atmospheric chemistry and aerosol physics in general circulation models. Beyond interactive computation of radiative feedbacks, this **on-line** approach presents the advantage of providing, for tracer transport, access to all the "physics" accounted for through "parameterizations" in circulation models, such as turbulent mixing in the planetary boundary layer or vertical transport by cumulus convection (*e. g.*Mickley et al., 1999; Shindell et al., 2001; Boucher and Pham, 2002; Hauglustaine et al., 2004). Similar approaches have been developed for the atmospheres of other planets like Mars (Lefèvre et al., 2004) or Titan (Rannou et al., 2002) where aerosols and chemical compounds have even a first order radiative impact on the atmospheric general circulation.

On-line models are often developed to be used in a climate mode (long integrations, far from initial state, usable only in terms of statistics). However, for the purpose of validation, it is useful that those models can be used in a configuration closer to chemistry transport models, with meteorological variables issued from observations or operational analysis. A general approach to this problem would consist in assimilating meteorological observations as currently done in operational meteorological centers. This generally turns out to be too heavy for current research applications. An alternative consists in using analysis or reanalysis of operational meteorological centers as if they were observations and assimilate them in the model (Jeuken et al., 1996). A simple way of doing this consists in adding a relaxation term in the general circulation model forcing the model to stay close to meteorological analyzes. This method is often referred to as **nudging**.

In the on-line approach, a number of meteorological fields such as large scale mass fluxes or eddy diffusivity must be "passed" to transport modules. If feedbacks on radiative transfer or cloud micro-physics are not taken into account, the transport modules can also

be **unplugged**: the required meteorological fields are archived in a first meteorological simulation and read afterwards. We will call this mode "unplugged" rather than "off-line" to avoid confusion with chemistry transport models. The unplugged version can also be integrated backwards in time to interpret a particular measurement at a station (Hourdin and Issartel, 2000). This mode is equivalent to the adjoint of the transport model which is provided without any further development (Hourdin and Talagrand, 2005; Hourdin et al., 2005).

Such capabilities have been implemented recently in the general circulation model LMDZ developed at Laboratoire de Météorologie Dynamique. This model includes a Zooming capability ("Z" of LMDZ) and has been chosen as the atmospheric component of an integrated climate model developed at Institut Pierre Simon Laplace in Paris (Marti et al., 2005) and used recently to produce climate change simulations for the fourth IPCC assessment report (Dufresne et al., 2005, see e. g.). LMDZ is used also to study the atmospheric chemistry of the Earth (Hauglustaine et al., 2004), Mars (Lefèvre et al., 2004) and Titan (Hourdin et al., 2004). The nudged and unplugged version has been used in the frame of the Comprehensive Test Ban Treaty to evaluate the efficiency of the global network of stations under deployment, which will monitor routinely the atmospheric radioactivity (Hourdin and Issartel, 2000).

The present paper pursues the following goals.

1. It presents in details the implementation of the tracer component in the LMDZ model. In that point, the paper follows a paper by Hourdin and Armengaud (1999) presenting the inclusion of finite volume schemes for large scale advection in LMDZ.

2. We present in details the zoom as well as the nudged and unplugged modes of LMDZ discussing the comparison with the classical off-line approach used in chemistry transport models.

3. Based on simulations of the European Tracer Experiment (ETEX), we evaluate the ability of the nudged and unplugged versions of LMDZ to predict the dispersion of a cloud of pollutant at continental scales.

4. The same context is used to test the sensitivity of the dispersion model to some parameters such as relaxation time constant for nudging or spatial resolution.

Results are discussed both in the context of climate modeling and environmental monitoring. In a companion paper (Coindreau et al., 2005), we show how the same nudged and zoomed version of a global model can be used to assess parameterizations of physical processes with respect to in-situ measurements.

2. Model description

a. *The LMDZ general circulation model*

LMDZ is derived from the LMD general circulation model first described by Sadourny and Laval (1984). In addition to several significant modifications in the "physical package" through time, the model has been recently recoded in a more organized and flexible manner. It includes in particular a zooming capability: longitudes and latitudes are fixed arbitrarily at the beginning of a simulation.

The dynamical part of the code is based on a finite-difference formulation of the primitive equations of meteorology (see e.g. Sadourny and Laval, 1984). The dynamical equations are discretized on a staggered longitude-latitude Arakawa C-grid (see e.g Kasahara, 1977). The C-grid can be presented as a node-centered finite volume grid: the scalar variables (pressure, temperature, humidity and tracers) are defined at the center of grid cells whereas wind components are defined at the interfaces. This dynamical code is widely used both for studies of the Earth climate (Krinner et al., 1997; Li, 1999; Li and Conil, 2003) and for the numerical simulation of the general circulation of other planetary atmospheres, in particular for Mars (Hourdin et al., 1993; Forget et al., 1999) and Titan (Hourdin et al., 1995).

The physical package of the LMDZ3 version used here is close to that described by Le Treut et al. (1994). The radiation scheme is the one introduced several years ago in the model of European Center for Medium-Range Weather Forecasts (ECMWF) by Morcrette: the solar part is a refined version of the scheme developed by Fouquart and Bonnel (1980) and the thermal infra-red part is due to Morcrette et al. (1986). Condensation is parameterized separately for convective and non-convective clouds. In the present version, convection is parameterized using the mass-flux scheme developed by Tiedtke (1989). A prognostic equation for condensed water is included (Le Treut and Li, 1991). The large scale transport of vapor and condensed water is taken into account with Van Leer (1977) finite volume scheme (see also Hourdin and Armengaud, 1999). As for the boundary layer, the model includes a classical local closure with a turbulent coefficient depending on the local Richardson number. The surface drag is computed according to Louis (1979). The model also includes a parameterization for dry convective adjustment.

b. *Nudging*

LMDZ can either be used in climate mode, without forcing, or nudged by analyzes or reanalyzes from

operational weather forecast centers. Meteorological fields X (wind, temperature, ...) are relaxed toward analyzed fields X^a by adding a non-physical relaxation term to the model equations:

$$\frac{\partial X}{\partial t} = F(X) + \frac{X^a - X}{\tau} \tag{1}$$

where F is the operator corresponding to computation of the partial time derivative of the meteorological variables in the model. The time constant τ can be different for the different variables and for different regions.

Meteorological analyzes are interpolated linearly in both space and time before computing relaxation.

c. *Software aspects*

Only the dynamical part of the model treats exchanges between model grid boxes in the three directions. The physical part is a juxtaposition of independent vertical columns. In the model coding, those two parts are also handled in a different and independent manner. In particular, the horizontal grid in the physical part is viewed as a dumb index so that exactly the same codes can be used either for a 1D or 3D numerical simulation, or in a sub-domain, for instance for parallel machines.

In the climate mode, the model requires in entry two files describing the initial state: one for the meteorological fields and one for the internal variables of the physical package. Additionally, a file containing time-evolving boundary conditions such as the sea-surface temperature is needed. An additional archive containing the time evolving analysis is required when nudging is invoked.

This structure is illustrated in Fig. 1

d. *Tracer transport modeling*

In on-line models, the transport of chemical species or aerosols is generally treated separately and sequentially with respect to other processes (chemical reactions, micro-physics, sources, etc...). This decomposition is sometimes called operator splitting. The transport part is derived for a conservative tracer, which means a trace species conserved along air trajectories, $dq/dt = 0$. It is this transport part which is presented below and evaluated in the present study.

1). The continuity equation

When implementing tracer transport in a circulation model, the distinction must be made between explicitly resolved large scale transport (at the scale of a grid box for instance) and unresolved and subgrid-scale motions which must be parameterized.

The decomposition between large scale and turbulent flow relies on the notion of ensemble average. The ensemble average $\overline{q}$ is defined as the mean of a quantity q taken over a set of random realizations of the atmospheric flow. From ergodic considerations, the confusion is generally made (it is the case here) between ensemble average, spatial average at a given scale or time average. For compressible flows, it is convenient (and often not clear in the relevant literature) to introduce an air weighted average $\tilde{q} = \overline{\rho q}/\overline{\rho}$ and the perturbation defined as the difference between a given realization and the mean $q' = q - \tilde{q}$, with the property that $\overline{\rho q'} = \overline{\rho q} - \overline{\rho}\tilde{q} = 0$

Taking the ensemble average of the conservation equation for tracer q

$$\frac{\partial \rho q}{\partial t} + \mathrm{div}\,(\rho \mathbf{v} q) = 0 \tag{2}$$

and noticing that

$$\overline{\rho \mathbf{v} q} = \overline{\rho}\tilde{\mathbf{v}}\tilde{q} + \overline{\rho \mathbf{v}' q'}, \tag{3}$$

leads to

$$\frac{\partial \overline{\rho}\tilde{q}}{\partial t} + \mathrm{div}\,(\overline{\rho}\tilde{\mathbf{v}}\tilde{q}) + \mathrm{div}\left(\overline{\rho \mathbf{v}' q'}\right) = 0 \tag{4}$$

The variables $\overline{\rho}$, $\tilde{\mathbf{v}}$ and $\tilde{q}$ are the large scale variables accounted for explicitly in numerical models. From now, they will be noticed ρ, $\mathbf{v}$ and q.

With those definitions, the continuity equation for the air

$$\frac{\partial \rho}{\partial t} + \mathrm{div}\,(\rho \mathbf{v}) = 0 \tag{5}$$

is formally the same for one realization or for the ensemble average.

2). Large scale atmospheric transport

Three groups of schemes are classically used for the representation of large scale advection: the Eulerian, Lagrangian, and semi-Lagrangian techniques.

In the Lagrangian schemes (Walton et al., 1988; Taylor et al., 1991), distinct air parcels, in which the tracers are assumed to be homogeneously mixed, are followed as they are displaced by the winds. Lagrangian schemes are simple in concept and are not a priori subject to spurious diffusion. Lagrangian models are used a lot for dispersion computations. Their application to global climate modelling is not straightforward because the concentration must be known at each time step everywhere and because of the difficulty of coupling Lagrangian trajectories with other physical processes. A review of these models is given by Pasquill and Smith (1983).

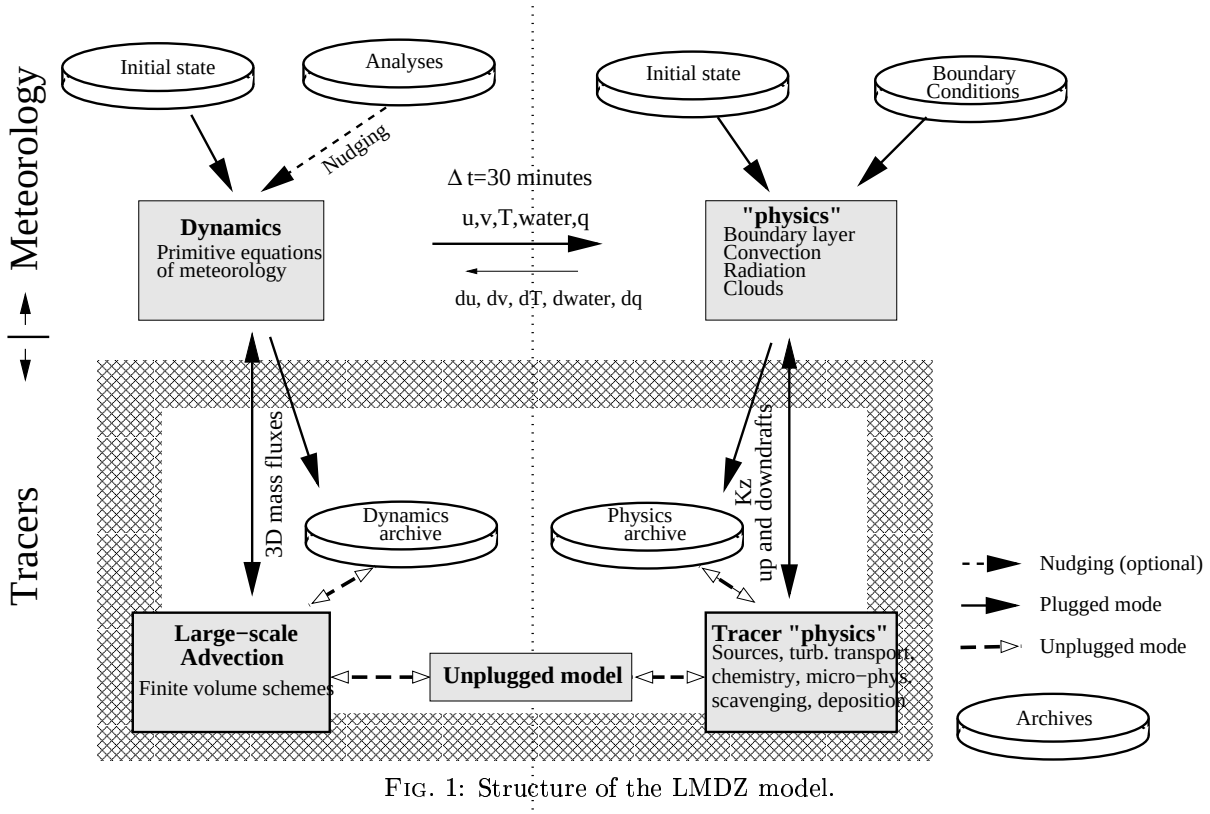

FIG. 1: Structure of the LMDZ model.

In the semi-Lagrangian approach (Robert, 1981; Williamson and Rasch, 1989), also named method of characteristics in numerical fluid dynamics, the solution on prescribed grid points is derived on the basis of Lagrangian backward integration over one time step. The success of this method is greatly dependent on the interpolation scheme used to reconstruct the tracer concentration at the origin of the backward trajectory (Staniforth and Côté, 1991). Semi-Lagrangian methods are not conservative and most chemical-transport models include a "fixer" applied after the advection calculation to correct deviations from exact mass conservation.

In grid point models, a variety of numerical algorithms have been developed to solve the advection equation, based on finite differences, finite elements or finite volume formulations (Rood, 1987). Recently, finite volume formulations (Godunov, 1959; Van Leer, 1977; Prather, 1986) have become quite popular.

Finite volume schemes have been implemented in the LMD general circulation model by Hourdin and Armengaud (1999). One should refer to this previous study to get detailed informations. In the present study, we use the Van Leer I scheme also named MUSCL in the literature. Finite volume methods are conservative by nature. Positivity and monotonicity can often be imposed. The counterpart is often a significant numerical diffusion (Lin and Rood, 1996). In the finite volume methods, the flux at an interface between two control volumes is computed as an integral over the upstream air which will cross the interface within the time step. It presents in that sense some similarities with semi-Lagrangian methods except that the latter compute local values rather than fluxes. In fact, there seems to be some convergence in the recent literature between the two approaches. Lin and Rood (1996) present finite volume methods as "Flux Form Semi-Lagrangian Transport Schemes" while some attempts are done to render semi-Lagrangian schemes conservative by introduction of flux computations (Yabe et al., 2001).

3). PHYSICAL PARAMETERIZATIONS

In LMDZ, the turbulent term div $\left(\overline{\rho \mathbf{v}' q'}\right)$ is treated as the sum of three distinct contributions as described bellow.

Boundary layer turbulence: The planetary boundary layer is treated in the standard version of LMDZ as a super-viscosity. The vertical transport of a scalar q writes

$$\overline{\rho w' q'} = -\rho K_z \frac{\partial q}{\partial z} \qquad (6)$$

with a mixing coefficient K_z which depends on the vertical wind shear and Richardson number following Laval et al. (1981).

Deep convection: Moist convection is handled by a so-called "mass-flux" scheme developed by Tiedtke (1989). This scheme divides an atmospheric column into three sub-columns: updraught, downdraught and environment. The updraught (resp. downdraught) is characterized by a mass flux $\hat{f}(z)$ (resp. $\check{f}(z)$). It exchanges air with the environment. This exchange is prescribed through an entrainment $\hat{e}$ (resp. $\check{e}$) and a detrainment $\hat{d}$ (resp. $\check{d}$). Mass conservation in the various compartments writes

$$\frac{\partial \hat{f}}{\partial z} = \hat{e} - \hat{d} \tag{7}$$

and

$$-\frac{\partial \check{f}}{\partial z} = \check{e} - \check{d} \tag{8}$$

with the convention that $\hat{f}$, $\hat{e}$, $\hat{d}$, $\check{f}$, $\check{e}$ and $\check{d}$ are all positive quantities and are equal to zero at the lower and upper boundaries. The fluxes in the updraught and downdraught are compensated by a flux in the environment $f_e = -\hat{f} - \check{f}$.

For tracers, the following approximations are made, consistently with the original scheme philosophy. The tracer is assumed to be always in a steady state regime both in the updraught and downdraught. In addition, the fractional area covered by the updraughts and downdraughts is assumed to be small enough so that the confusion can be made between the mean concentration in the model box and that in the environment of the convective tower ($q_e = \tilde{q}$ or q).

In this context, the tracer concentration in the updraught $\hat{q}$ is given by

$$\frac{\partial \hat{f}\hat{q}}{\partial z} = \hat{e}q - \hat{d}\hat{q} \tag{9}$$

with a similar equation for the downdraught

$$-\frac{\partial \check{f}\check{q}}{\partial z} = \check{e}q - \check{d}\check{q} \tag{10}$$

Finally, the total turbulent flux is given by

$$\overline{\rho w' q'} = \hat{f}\hat{q} - \check{f}\check{q} - (\hat{f} - \check{f})q \tag{11}$$

In order to ensure numerical stability, the various transport terms (of the form fq) in those equations are handled by a first order upstream scheme. The numerical diffusion is not a problem there because the physical process is diffusive by itself and because the numerical errors introduced are probably much smaller than the uncertainty on the mass fluxes themselves.

Lateral mixing: In addition to the parameterizations of vertical transport by boundary layer turbulence and cumulus convection, used in the standard version of the model, we added, for sensitivity experiments, a lateral diffusion based on a simple Laplacian operator with constant eddy diffusivity

$$\frac{\partial q}{\partial t} = K_h \Delta q \; . \tag{12}$$

4). UNPLUGGING:

The large scale and parameterized transport are computed sequentially. On the one hand, the large scale mass fluxes issued from the dynamical code are used to compute large scale advection of an arbitrary number of constituents. On the other hand, tendencies associated with turbulence and convection are computed in the physical part. In the plugged version, the large scale mass fluxes on the one hand, and sub-grid physical parameters on the other hand, are directly passed to the tracer modules at each time step (Fig. 1). In the unplugged mode, the mass fluxes and physical parameters needed for transport are read in a meteorological archive created in a previous meteorological simulation.

The unplugged version of LMDZ, when driven by meteorological archives produced during a nudged simulation, presents similarities with off-line chemistry transport models. The difference is that, in classical chemistry transport models, analyzed fields are used directly in the model and additional parameterizations must be developed for subgrid-scale mixing. This may cause spin-up problems due to the unbalance between large-scale fields and parameterizations. Here, the physical parameterizations are run interactively with the large scale dynamics and only parameters for tracer transport are passed to the unplugged model.

3. ETEX-1 experiment

a. *Description*

For model evaluation, we use results of the ETEX-1 experiment. On 23 October 1994, 340 kg of the insoluble gas Perfluoro-Methyl-Cyclo-Hexane (PMCH) were emitted continuously during 12 h starting at 4 p.m. (T0) at the top of a 8 m high tower located in Monterfile, some 30 km from Rennes in France. The meteorological situation, a strong and maintained westerly to south-westerly flow, was chosen in order to maximize detection at the 168 observing stations mainly located in the north of western Europe.

Fig. 2 shows the time evolution of surface concentrations of PMCH. Maps are reconstructed from sta-

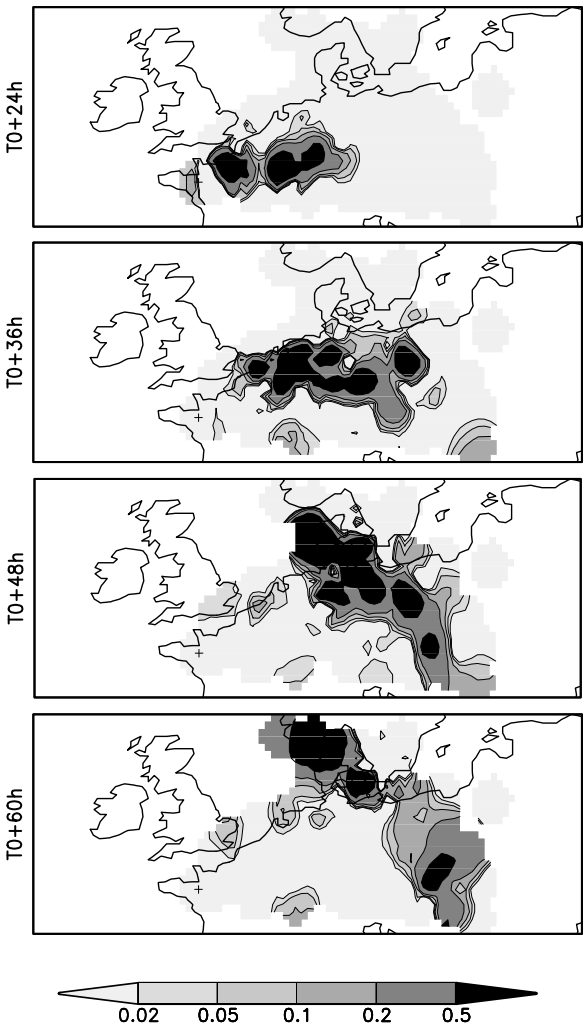

FIG. 2: Measured PMCH plume (in ng m^{-3}) at 24, 36, 48 and 60 hours after release time (T0). Maps are reconstructed from station data using Cressman (1959) algorithm.

tion data using the Cressman (1959) approach as implemented in the GRADS graphical package. At T0+12h, PMCH is detected in France and in a few German sites. Then, the plume moves eastward through Germany. At T0+48h, it stretches from the West coast of Sweden in the North to Hungary in the South. At T0+60h, the eastward motion of the cloud was blocked and the cloud stretched from Bulgaria to Norway.

b. *Statistical analysis*

In order to analyze the model performances, we adopted the statistical indices used by the Model Evaluation team of ETEX (Van Dop and Nodop, 1998; Klug et al., 1992) :

The bias, defined as $b = \frac{1}{N}\sum_i (P_i - O_i)$ where P_i and O_i are respectively the model prediction and observation for measurement i, can be defined at given time for all the stations or at given station for all times or for all stations and all times.

The FMT or figure of merit in time is defined, when the simulated and observed time-series are plotted on the same graph, as the ratio of the overlap area between the two curves to the total area defined by the envelope of the two curves. The FMT, which varies from 0 to 100%, depends both on the time shift between the two signals and on their relative magnitudes. Following the intercomparison work, 11 stations were selected, among those with no gap in the data, for temporal analysis. Those stations form two arcs at T0+24h and T0+48h on the cloud trajectory (cf. Fig. 3).

The FOEX, factor of exceedence is defined as $FOEX = 100\,(\frac{N(P_i>O_i)}{N} - 0.5)$ where $N(P_i > O_i)$ is the number of measurements for which the model prediction is larger than observation and N is the total number of points. FOEX ranges from -50% and 50%.

The FA2 and FA5, factor of agreement within a factor 2 or 5, represent the percentages of simulated values within a factor of 2 and 5 from the observed values.

4. Simulations and analysis

a. *Control simulation*

The nominal horizontal grid used for ETEX-1 simulations (Fig. 3), with 96 points in longitude and 72 in latitude, reaches a mean resolution of about 120×150 km^2 in the center of the zoom over Europe. A complete description of the zoom function and the choice of parameters retained for the control simulation are given in Appendix A.

On the vertical, the model uses a classical hybrid $\sigma - p$ coordinate (see *e. g.* Simmons and Burridge, 1981): the pressure P_l in layer l is defined as a function of surface pressure as

$$P_l = A_l P_s + B_l \tag{13}$$

The values of A_l and B_l are chosen in such a way that the $A_l P_s$ part dominates near the surface (where A_l reaches 1), so that the coordinate is following the surface topography, and B_l dominates above several km, making the coordinate equivalent to a pressure coordinate there. We use here the current vertical grid

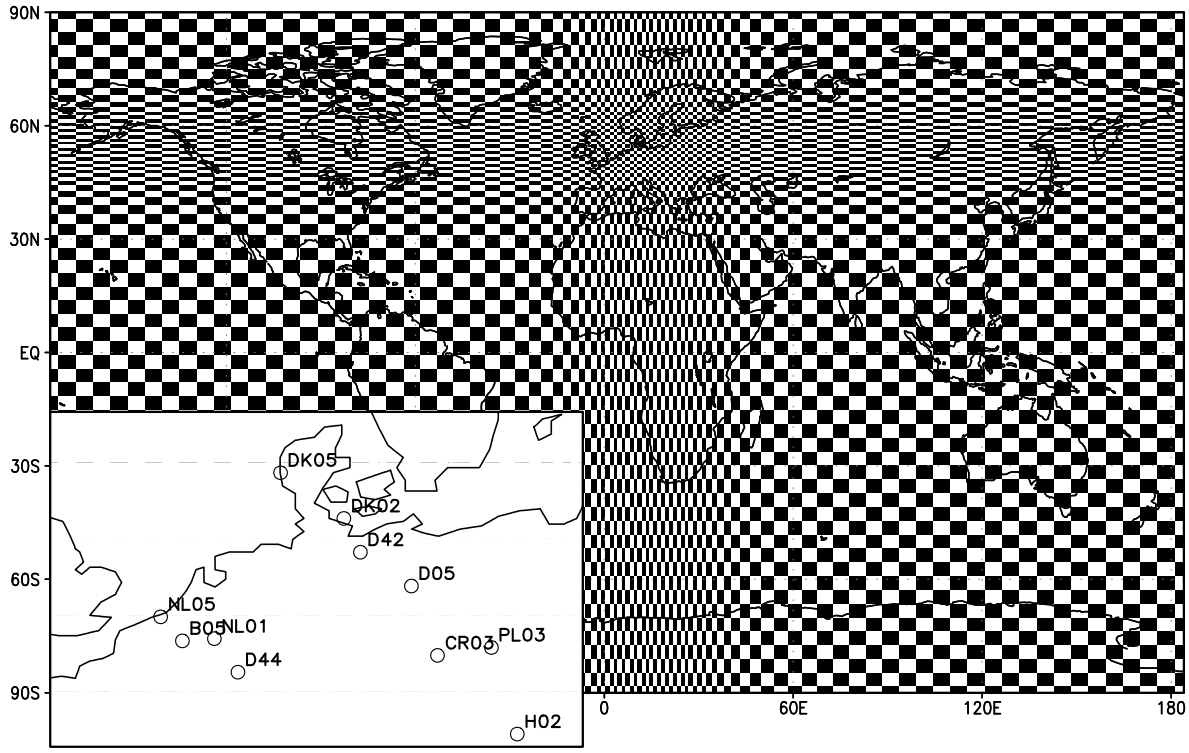

FIG. 3: LMDZ grid with 96x72 points and a zoom over Europe and the location of the 11 stations selected for temporal analysis.

of LMDZ with 19 layers. Approximate altitudes above the surface are 70, 240, 490, 880 m for the first four layers and 1.5, 2.3, 3.5, 5.1, 7.1, 9.2, 11.2, 12.7, 14.4, 16.3, 18.6, 21.2, 24.9, 29, 40 km for the others.

In order to avoid spin-up problems, the model is nudged by ECMWF analysis during the four days preceding the campaign. The final state of this simulation, 16 hours before release, is used as an initial state for the ETEX simulation. Wind and temperature fields are also relaxed toward ECMWF analysis with a relaxation time constant of 3 hours. The meteorology is computed with a time step of 1.5 minutes. Large scale advection and tendencies associated to turbulence in the planetary boundary layer are computed with a time step of 30 minutes.

Fig. 4 shows the simulated PMCH plume at T0+24, 36, 48 and 60 hours. In order to be more consistent with observations, rather than plotting directly the simulated plume from the gridded variables, we first compute the time series of concentrations at each station (using simply the simulated concentration in the grid box where the station is located) and then reconstruct the plume with the Cressman algorithm. Fig. 5 shows, for one particular time (T0+48h, third panel of Fig. 4), the same plume issued directly from the LMDZ grid.

The observed and simulated time series of concentrations are shown in Fig. 6 for the 11 selected stations together with the corresponding FMTs. According to the scatter diagram (Fig. 7), 25 % of the simulated concentrations are within a factor 2 of measured concentrations and 48 % within a factor of 5.

b. *Comparison with other models*

28 models from 24 different organizations – mainly national meteorological services and nuclear safety institutions – have participated to the ETEX experiment (Graziani et al., 1996). Three groups of models can be identified: the group of Gaussian puff models (twelve models), that of Eulerian models (six models) and the group of Lagrangian particle models (ten models). The horizontal resolution is largely variable and seems not to be correlated with the kind of dispersion model.

According to the evaluation conducted by the Model Evaluation Team of ETEX and given by Klug et al. (1992), there is generally a satisfactory agreement between model results and measurements. Retaining the same criteria, LMDZ ranges in the category of good models.

In Fig. 8, the FMTs obtained with LMDZ for the 11 selected stations are compared with the results published after the campaign by Graziani et al. (1996).

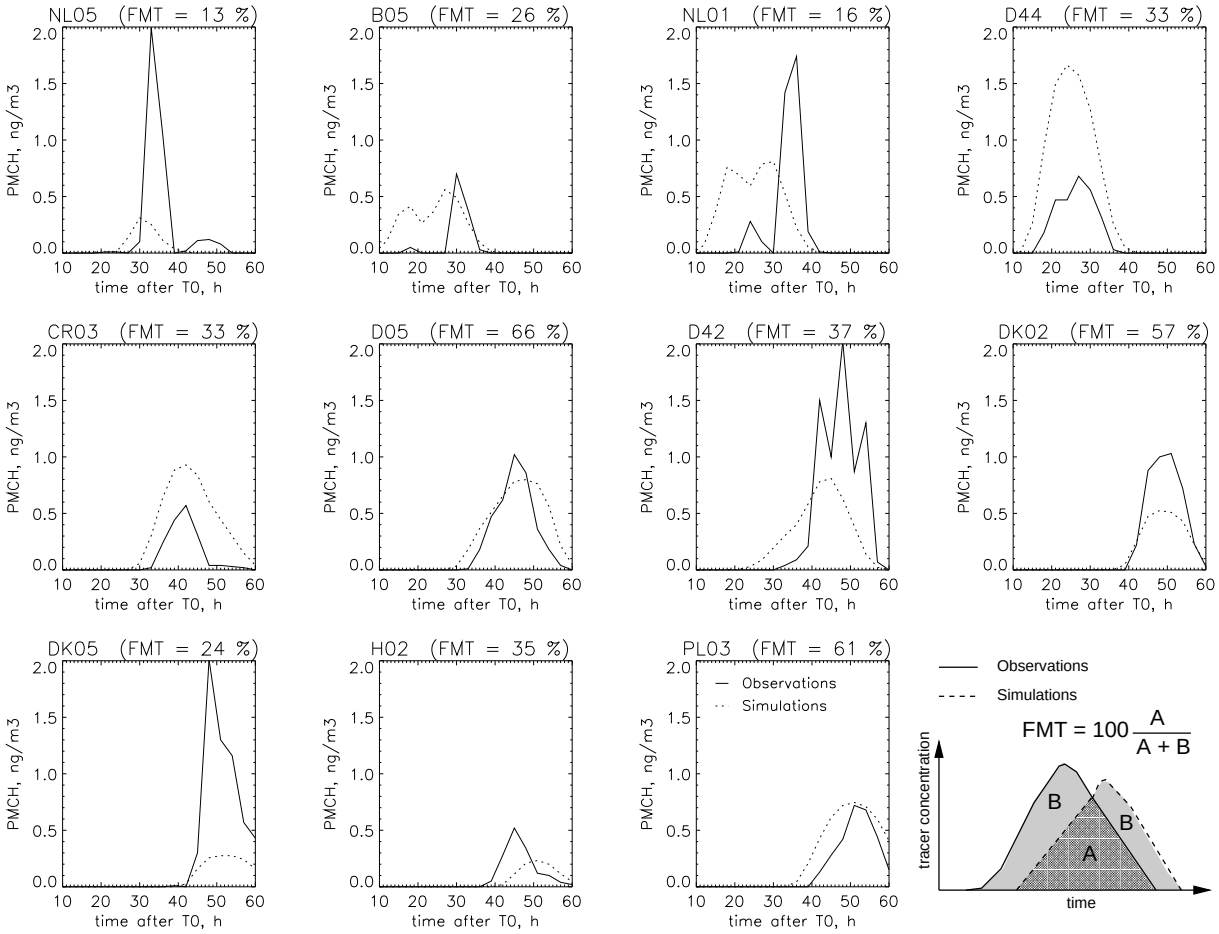

FIG. 6: Time evolution of the concentration of PMCH (in ng m^{-3}) as observed and simulated with LMDZ (control simulation) and associated FMTs.

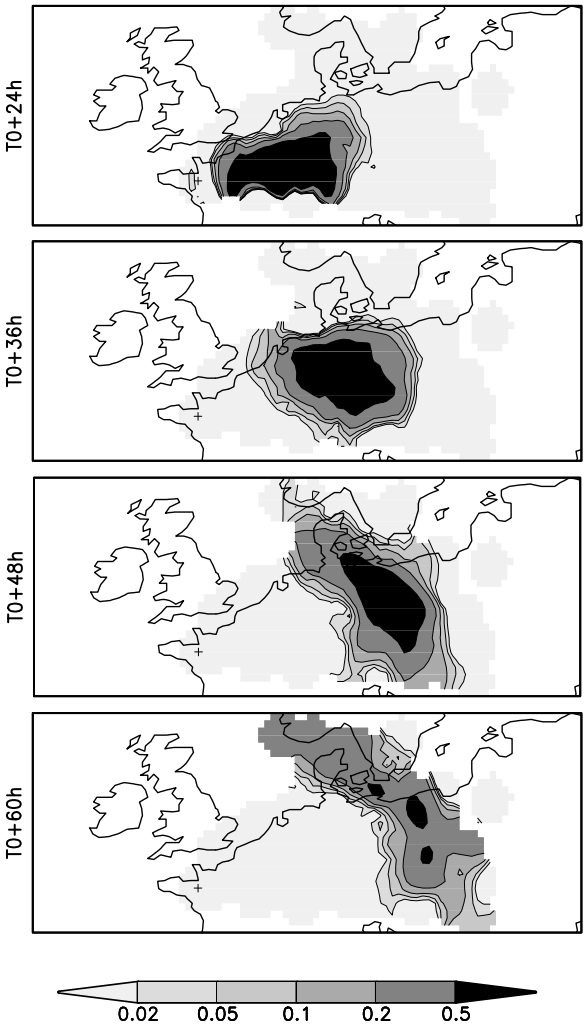

FIG. 4: Simulated PMCH plume (in ng m^{-3}) at 24, 36, 48 and 60 hours after release.

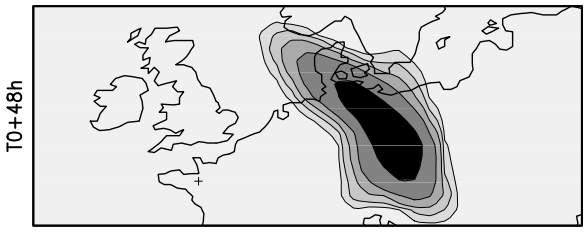

FIG. 5: The simulated PMCH plume at T0+48h (ng m^{-3}) with the direct output on the model grid (bottom).

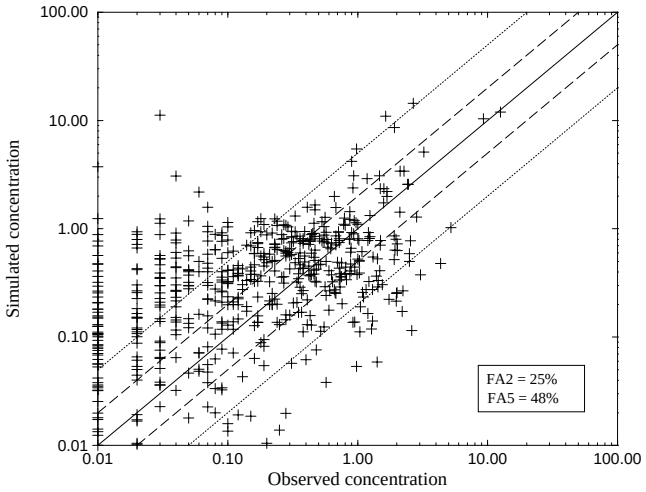

FIG. 7: Global scatter diagram for the simulated (control simulation) versus observed PMCH concentrations (ng m^{-3}).

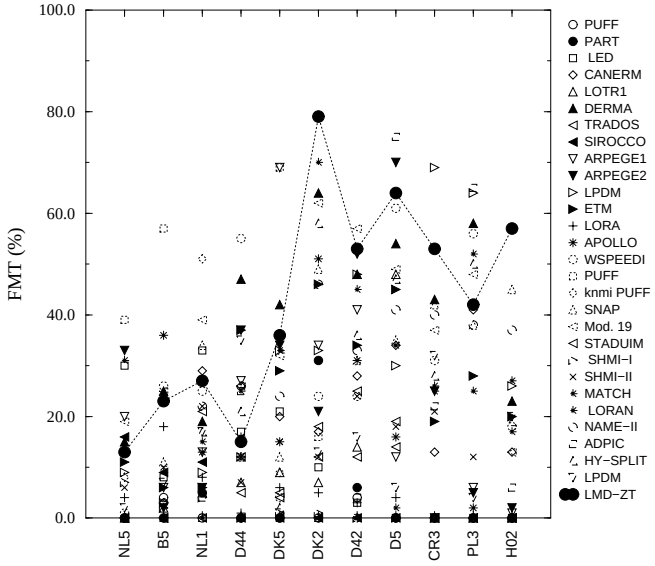

FIG. 8: Comparison of the FMTs of LMDZ (control simulation) with that obtained from intercomparison studies during ETEX.

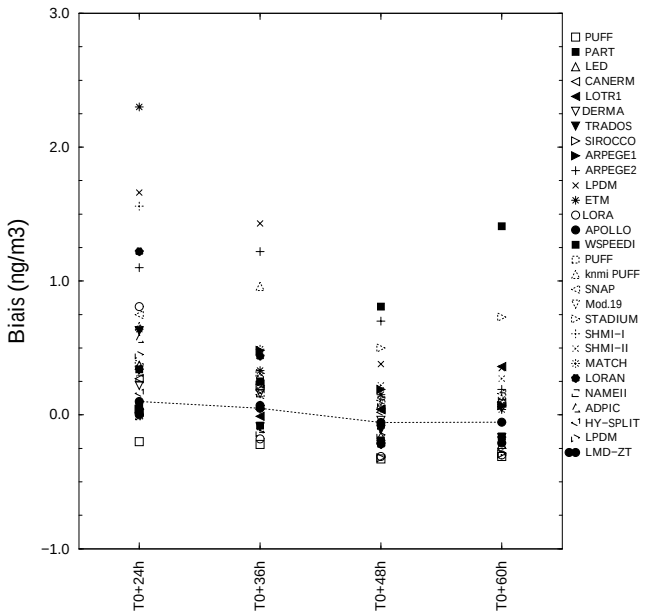

FIG. 9: Comparison of the bias of LMDZ and other models at T0+24, 36, 48 and 60 h.

Values of global parameters are compared in Table 1. The factors of agreement range between 13 and 34% for FA2 and 27 and 48% for FA5. The FOEX varies from -29 to 26% and the mean bias from -0.27 to 12.2 ng m^{-3}. When comparing LMDZ with the other models, the FA2 (25%) and FOEX (14%) factors are in the average and the FMTs, FA5 (48%) and mean bias (0.07 ng m^{-3}) are relatively good. Note that the intercomparison study is not so recent and new versions of the various models may of course give better results.

Models	FA2 %	FA5 %	FOEX %	Bias ng/m^3
PUFF	26	27	-29	-0.27
PART	28	29	-23	1.6
LED	19	25	-7	0.08
CANERM	26	39	5	0.16
LOTR	25	29	-11	0.12
DERMA	23	40	27	0.44
TRADOS	29	30	-29	0.59
SIROCCO	28	29	-28	0.06
ARPEGE1	15	27	16	1.03
ARPEGE2	13	26	25	1.36
LPDM	19	35	31	1.58
ETM	15	32	15	0.48
LORA	26	33	-21	0.08
APOLLO	30	36	-17	0.35
WSPEEDI	30	45	4	-0.06
PUFF	28	31	-19	1.1
knmiPUFF	27	30	-22	0.27
SNAP	34	44	-2	0.24
Mod.19	18	36	26	0.17
STADUIM	32	36	-17	0.44
SHMI 1	26	39	-22	6.46
SHMI 2	28	34	-7	0.62
MATCH	26	39	14	0.64
LORN	26	30	-11	0.06
NAME 2	35	47	4	0.35
ADPIC	33	42	-12	1.97
HY-SPLIT	34	43	-5	12.2
LPDM	26	31	-16	-0.08
LMDZ	25	48	14	0.07

Table 1: Global comparison between LMDZ and other models

c. *Sensitivity to model parameters*

We now evaluate the sensitivity of the model results to important parameters such as nudging time constants, archiving frequency for the unplugged mode or spatial resolution.

1). SENSITIVITY TO RELAXATION TIME CONSTANT

A series of plugged simulations nudged with different relaxation time constants were performed. Fig. 10 shows for each simulation the values of the FMT for the 11 selected stations.

Simulations are closer to observations for the smallest relaxation time constants. Very short time constants force the wind to match closely meteorological analysis, themselves constrained by observations during the whole period, especially in this part of the world. Sensitivity to the relaxation time constant is in fact weak for values smaller than 3 hours. Differences start to be significant for relaxation time constants larger than 6 hours.

This capacity of the model to follow closely the observed situation even for time constants of a few hours enables one to use the nudged model as a tool for evaluation of physical parameterizations as discussed in part II of this paper. Indeed, the temporal scale of several physical phenomenons is of a few hours or less (cloud thermodynamics, boundary layer dynamics, or to a lesser extent, deep convection). With a relaxation time constant of a few hours, the synoptic situation is strongly forced but a certain degree of freedom is left to the parameterizations.

Note that it could happen that the results are better with a constant of a few hours than with a much shorter one, for example if the physics of the model used for the analysis differs significantly from that of

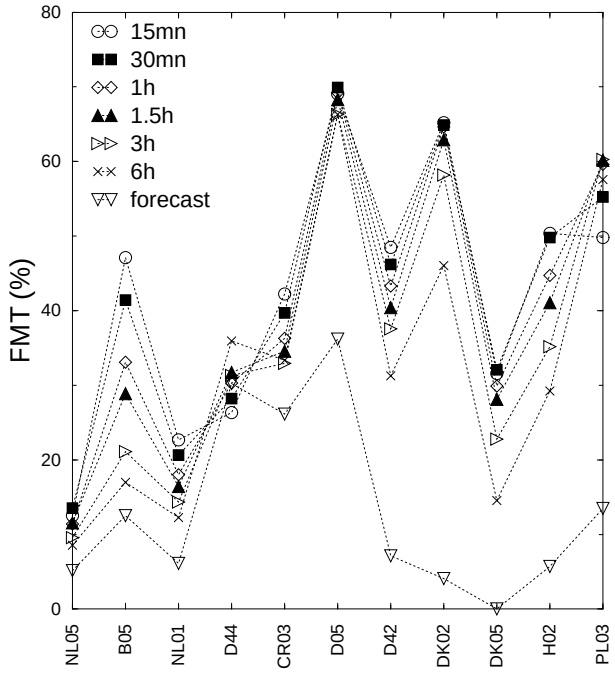

FIG. 10: Sensitivity to relaxation time constant (τ). FMTs for the 11 stations and for simulations with $\tau = 0.25, 0.5, 1, 1.5, 3, 6$ h and for a forecast simulation ($\tau = \infty$).

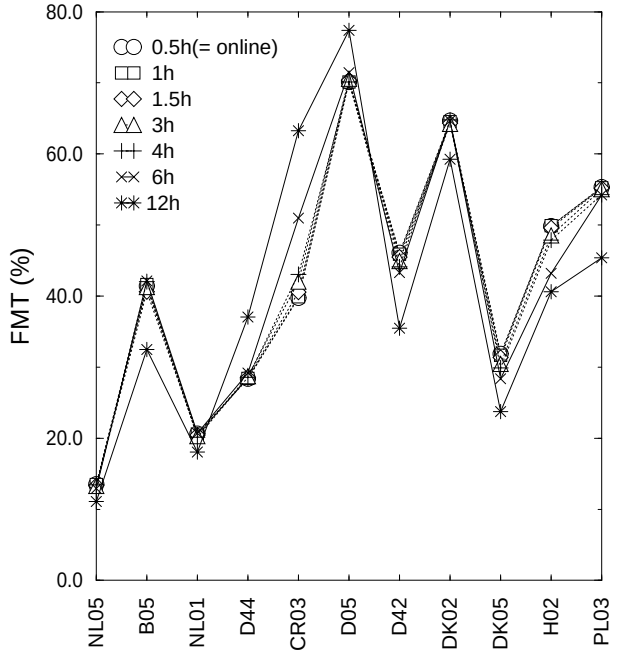

FIG. 11: Sensitivity to archiving frequency. Values of FMTs for each of the 11 stations and for unplugged simulations using the archives with 0.5, 1, 1.5, 3, 4, 6 and 12 hours.

the nudged model, either because the nudged model has a better physics or just because the analyzed fields are incompatible with the physics of the nudged model. For instance a vertical temperature profile which would be considered slightly unstable in the model used to produce the analysis but slightly stable in the nudged model could result in an underestimated mixing in the latter. Off-line models face in fact a similar spin-up problems. ETEX is not a good case to illustrate this point since the simulations appear to be only weakly sensitive to the physical parameterizations (results not shown).

For the next simulations, a relaxation time constant of 3 hours was retained.

We also performed a forecast simulation as follows. As for the other simulations, the model was first nudged by ECMWF analysis during the four days preceding the campaign. The final state of this simulation, 16 hours before the release, was used as an initial state for a simulation with no relaxation. As expected, the forecast simulation is farther from observation. However, at T0+24h (stations NL05, B05, NL01, D44), thus 40 hours after the beginning of the forecast simulation, the results look still reasonable.

2). SENSITIVITY TO ARCHIVING FREQUENCY

Unplugged versions of LMDZ are widely used for validation aspects and for backward transport computations (Hourdin and Issartel, 2000).

For practical reasons, the meteorological fields can generally not be archived at each time step of the transport computation. Mass fluxes are thus cumulated in time and stored typically each 3 or 6 hours. In the unplugged model, this storage time step must be split back into several shorter time steps for transport computations. For instance, if the time-step of the archive is of 6 hours and the time-step of advection is 1 hour, the same mass flux is used during 6 consecutive time-steps. Because mass fluxes are properly cumulated and split, the plugged and unplugged modes give identical results if the meteorological fields are actually constant between two storages.

We performed a series of plugged and unplugged simulations with different archiving frequencies (Fig. 11). The first plugged simulation was run with a unique time step of 30 minutes for large scale advection, parameterized vertical transport and archiving. The corresponding unplugged simulation gives exactly the same results. In fact, for archiving periods up to 4 hours, the results are almost superimposed. The difference starts to increase when the archiving frequency

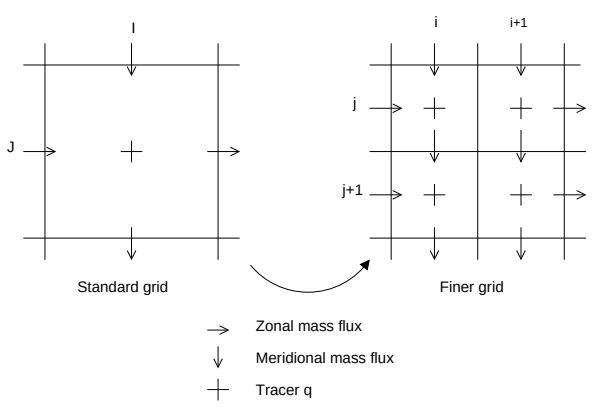

FIG. 12: Illustration of the mesh splitting.

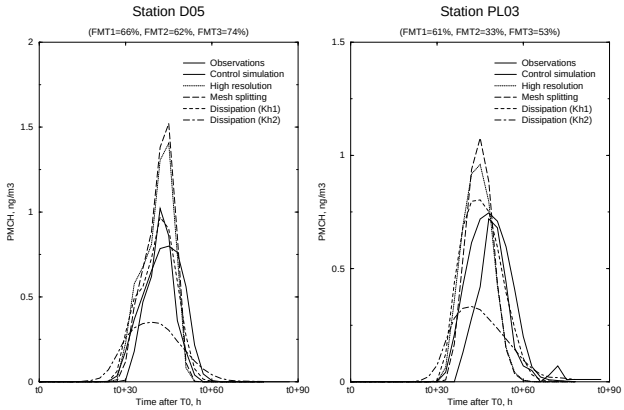

FIG. 13: Time evolution of the concentration of PMCH as observed and simulated with different configurations of LMDZ: control simulation, plugged high resolution simulation, high resolution simulation with mesh splitting (using the meteorological archive from the control simulation). The plugged high resolution simulation is also run with an additional lateral diffusion with diffusivity $K_{h1} = 10^5$ m^{2}s^{-1} and $K_{h2} = 10^6$ m^{2}s^{-1}. Associated FMTs measuring the distance from observations are also given for the control (FMT1), high resolution (FMT2) and $Kh1$ (FMT3) simulations.

is greater than 12 hours.

We retained an archiving frequency of 3 hours for the following simulations.

Note however that ETEX-1 is probably once again a favorable case for long storage time steps with a meteorology dominated by a well established westerly flow. With a greater importance of local meteorology, a more frequent storage could be required. This could be particularly important for instance with a strong diurnal cycle over continents, correlated with the diurnal cycle of surface emissions, as is the case for CO_2 on vegetal covers.

3). SENSITIVITY TO HORIZONTAL RESOLUTION

In order to test the sensitivity of transport to horizontal resolution, we performed two simulations with a finer grid (60x75 km in the center of the zoom).

In the first one, both the meteorology and the transport are computed on a finer grid. In the second one, we use the meteorological archive from the control simulation to perform an unplugged simulation on a grid twice as fine in each horizontal direction: the grid cells are split by two in each horizontal direction as illustrated in Fig. 12. Where interfaces coincide, the horizontal flux of the coarse grid is used directly on the finer one. For new interfaces, inside a cell of the coarse grid, mass fluxes are interpolated linearly. The same vertical mass flux is used for the four sub-cells.

Refining the grid for transport is an alternative to the use of less diffusive schemes (Hourdin and Armengaud, 1999) and allows to have more detailed representation of sources.

Corresponding time series are shown in Fig. 13 for two particular stations (D05 and PL03). As expected, a finer grid results in a less diffuse plume, which translates at the stations into higher tracer concentrations with a smaller extent in time.

Simulations	FA2 %	FA5 %	FOEX % X	Bias ng m^{-3}
Control simulation	25	48	14	0.07
Mesh splitting	24	46	17	0.08
High resolution	23	45	11	0.15
Diffusion (K_{h1})	26	47	15	0.1
Diffusion (K_{h2})	23	44	15	-0.08

Table 2: Sensitivity to horizontal resolution. Values of the global parameters for the different LMDZ simulations. FA2, FA5 and FOEX are in % and Bias in ngm^{-3}

The two simulations with a finer grid show generally quite similar results suggesting that the sensitivity to resolution comes from the transport computation and source representation rather than from meteorology.

The model at high resolution tends to overestimate the values of the peak concentrations suggesting an underestimation of the effective diffusion of the tracer. The overall performance of the high resolution simulations is in fact somewhat below that of the control simulation as can be seen from the FMTs of the 11 selected stations Fig. 14, from the global parameters in Table 2 as well as from the FMT maps of Fig. 15.

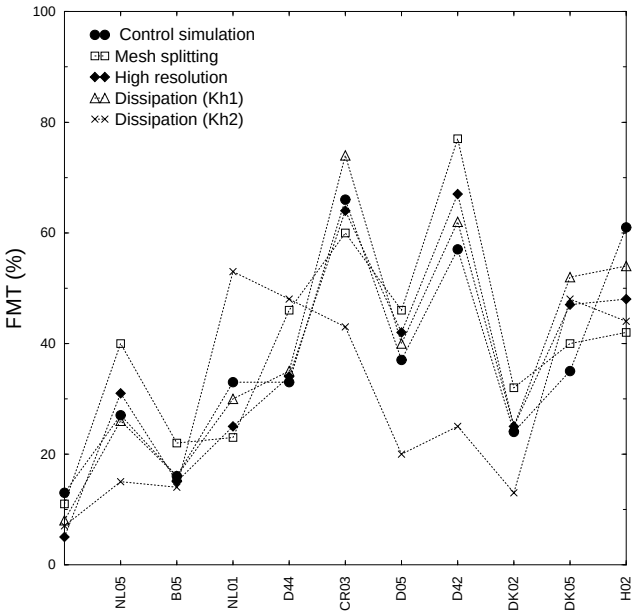

FIG. 14: Values of FMTs for each of the 11 stations for the plugged simulation at low horizontal resolution, for the unplugged simulation where transport is computed on a finer grid using archives of the plugged control simulation, for the plugged simulation at high horizontal resolution and for the plugged simulation at high horizontal resolution with lateral mixing coefficient of diffusion of $K_{h1} = 10^5\ m^2 s^{-1}$ and $K_{h2} = 10^6\ m^2 s^{-1}$.

The results can indeed be slightly improved by adding a lateral diffusion with a diffusivity K_h of about 10^5 m^2 s^{-2}. For this value, the shape of the curves at the two stations of Fig. 13 is close to that of the control simulation. This simulation results in larger FMTs both in the center and in the northern part of the ETEX observation domain (Fig. 15). The overall performance (Table 2) is however not better than that of the control simulation.

The model clearly starts to overestimate the lateral diffusion for $K_h \geq 10^6$ m^2 s^{-2}. Comparing the biases in the last three lines of Table 2, it appears that lateral diffusion tends to decrease the mean surface value, probably by exporting more tracer outside the observation domain.

4). SENSITIVITY TO METEOROLOGICAL ANALYZES

Finally the sensitivity of the results to the meteorological analyzes was tested by comparing two simulations using either ECMWF or NCEP analyzes for nudging.

The results are quite instructive.

For the stations on the first arc (NL05, B05, NL01

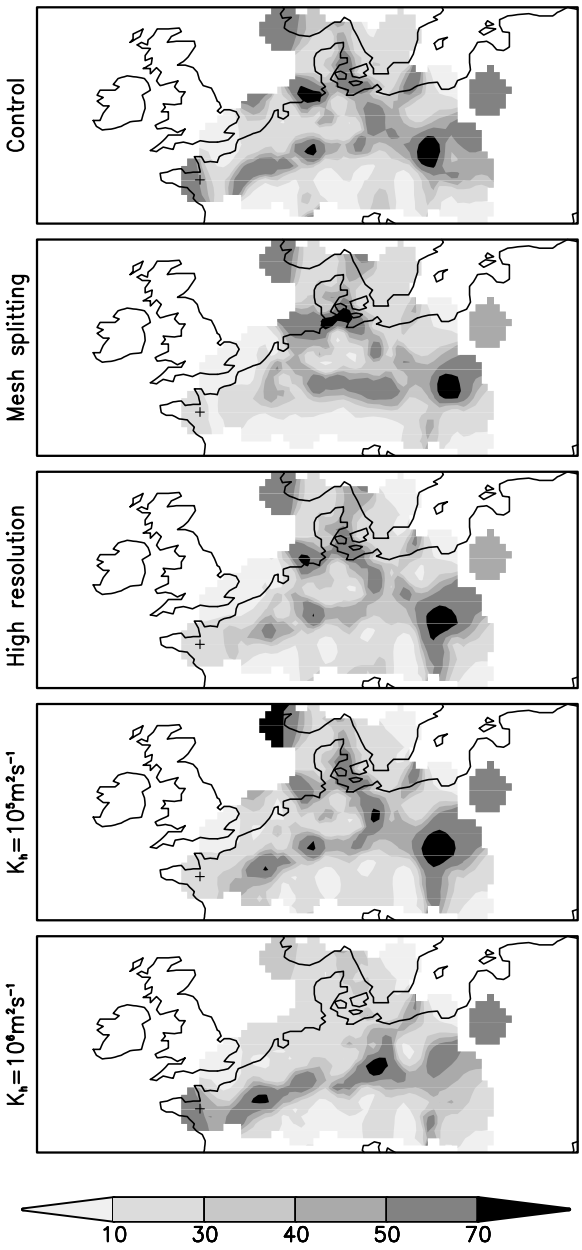

FIG. 15: FMT maps, for the plugged simulation at low horizontal resolution, for the unplugged simulation where transport is computed on a finer grid using archives of the plugged control simulation, for the plugged simulation at high horizontal resolution and for the plugged simulation at high horizontal resolution with lateral mixing coefficient of diffusion of $K_{h1} = 10^5$ m^{2}s^{-1} and $K_{h2} = 10^6$ m^{2}s^{-1}. The maps are reconstructed from station FMTs using the Cressman (1959) approach.

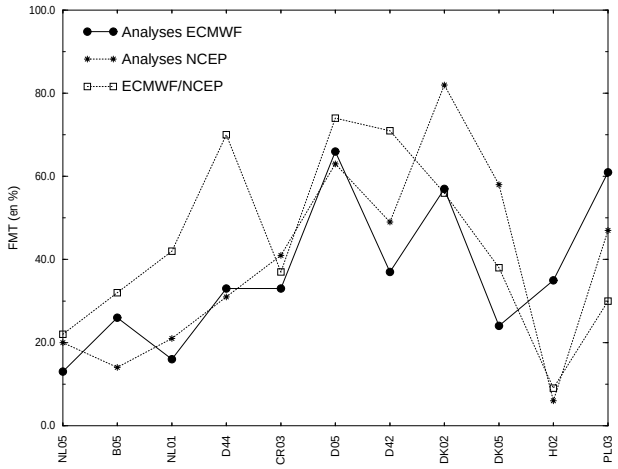

FIG. 16: Sensitivity to meteorological analyzes. Values of FMTs for the 11 stations computed between the simulation nudged by ECMWF and observations, between the simulation nudged by NCEP analyzes and observations and between the two simulations.

and D44) both simulations give comparable FMTs (see Fig. 16), whereas the results for the second arc are more different as could be expected from the longer delay between emission and detection.

For the second arc also, the FMTs measuring the difference between the two simulations are on average the same as that between each simulation and observations. Thus, for this second arc, the discrepancy between model and observations is of the order of the uncertainty coming from the analyzed wind fields. For the first arc, the situation is different. The discrepancy between both is much less than the discrepancy between model and observation suggesting a deficiency of the LMDZ model.

It is noteworthy that the envelope of the FMTs in Fig. 8 for all models seems to be strongly correlated with the FMT measuring the difference between the simulations nudged by ECMWF and NCEP analysis (squares in Fig. 16).

5. Discussion and conclusions

ETEX was used as a test case for validation of the tracer version of the LMDZ general circulation model, nudged by meteorological analysis.

Experiments such as ETEX are interesting for model evaluation since the source is well known and because the surface concentrations are well sampled. It also offers an opportunity of comparison with other models on well defined cases.

The ETEX simulations presented here place the transport version of LMDZ in the group of good dispersion models when adopting the criteria proposed by Klug et al. (1992) and Graziani et al. (1996). As expected, the transport simulated with finite volume methods is less diffusive if a finer grid is used, even if the refined grid is used for the dispersion calculation only, in the unplugged mode. The results in fact suggest that, for a mesh finer than 100×100 km^2, the model starts to underestimate lateral diffusion: addition of a lateral diffusion with a diffusivity of about 10^5 m^2 s^{-2} improves somewhat the results with the finest grid. This needed lateral dispersion, in the lower troposphere, could be related to an underestimation of the wind variability in the analysis and model, linked for instance to the effect of unresolved orography (note that the PMCH plume crosses a number of mountain chains, poorly represented, even with a 60×60 km^2 mesh). This could be consistent with an improvement observed in a dispersion model when using ECMWF analyzes at a higher resolution of 0^o5 x 0^o5 against 1.125×1.125 as in our simulations (Van Dop and Nodop, 1998).

It is noteworthy that, for estimation of surface concentrations at horizontal scales of around 1000 km, a second order finite volume scheme with a grid mesh of 100×100 km^2 behaves satisfactorily well, even for the most challenging case of a point source.

ETEX was also used to assess the different tools developed around the tracer version of LMDZ (nudging, unplugged mode). With relaxation time constants and archiving frequencies up to several hours, the model does not depart much from the control simulation. Even for larger values, the discrepancy is smaller than the difference obtained when changing the meteorological analysis. Comparing the FMTs obtained for the various sensitivity experiments presented here, as well as those obtained for other models (Table 1), with the FMTs measuring the discrepancy between the LMDZ simulation nudged by NCEP and ECMWF analyzes suggests that, for the best dispersion models, the performance is limited by the uncertainties on the analyzed wind fields.

Another limitation of the ETEX-1 experiment is the weak sensitivity to the parameterized physics. For instance, simulations of Rn^{222} surface concentrations performed with LMDZ show a strong sensitivity of the simulated diurnal cycle to the parameterization of the vertical turbulent transport in the convective boundary layer (Idelkadi, 2002). The same tests show almost no effect on ETEX results (not shown).

For dispersion calculations, the use of a global grid with zoom capability is both a drawback because it increases significantly the model cost for the same resolution in the region of interest, and an advantage.

For practical applications, the location of the source (for direct simulations with a declared source) or retro-source (for interpretation of a suspicious measurement at a station for instance) is generally known, but the distance to which the pollutant will propagate (for direct simulation) or the distance from which the pollutant has been emitted (for a retro-simulation) is not known a priori. The global grid avoids the problem of a priori determination of a limited area. By zooming the model grid around the source or retro-source, the model will give a precise answer close to the source and a coarser description farther, in a region where the intrinsic diffusivity of atmospheric transport will anyway result in diffuse results, as clearly visible on the observed and simulated ETEX plumes.

The global grid is also interesting of course when analyzing the results of a global network as the radio-nuclide network deployed in the frame of the Comprehensive Test Ban Treaty (Hourdin and Issartel, 2000).

The original motivation for including tracers in the LMDZ climate model was the study of the coupling between climate and chemistry or aerosol micro-physics. In this context, the zooming and nudging capabilities are used to validate the chemical, micro-physical or transport modules in the context of terrain campaigns or short time series. This approach can be used in fact to assess physical parameterizations themselves, as shown in part II of this paper.

Acknowledgments

This study was funded by Centre National de la Recherche Scientifique (CNRS) and Commissariat à l'Energie Atomique (CEA). Simulations have been run on a NEC-SX5 at the IDRIS computer center of CNRS. Graphics have been made with the user friendly and public domain graphical package named GrADS originally developed by Brian Dotty (COLA, support@grads.iges.org).

A. The zoom definition

The zoom is specified in both horizontal directions by applying a stretching function to the longitudes and latitudes of the regular grid. The function, based on hyperbolic tangents, is designed so as to obtain a near constant resolution both inside and outside the zoom.

The longitudes X_i of the regular grid are simply prescribed as $X_i = -\pi + 2\pi(i-1)/IM$ where $i = 1, ..., IM$ is the point index.

The longitude x of the zoomed grid is defined implicitly by imposing a stretching factor

$$X'(x) = g(x) = \gamma + (\epsilon - \gamma) G(x - x_0, \delta, \tau) \qquad (14)$$

where

$$G(x, \delta, \tau) = \frac{1}{2}\left\{1 - \tanh\left[\frac{\tau(\delta - |x|)}{|x|(\pi - |x|)}\right]\right\} \qquad (15)$$

defined for x in $[-\pi, \pi]$, takes values between 0 at the zoom center and 1 far from the zoomed region. The stretching factor is symmetric around the central longitude x_0. δ is the half-width of the zoomed region. The zooming factor γ is defined as the ratio between the longitudinal resolution of the regular grid, $2\pi/IM$, and the effective resolution at the center of the zoom, and τ controls the stiffness of the transition at the frontier of the zoomed region.

The elongation factor ϵ outside the zoom, ratio of the effective resolution to that of the regular grid, is found by imposing that the regular and zoomed coordinates coincide at x_0 and $x_0 \pm \pi$ so that

$$\pi = \int_{x_0}^{x_0+\pi} g(x)\, dx = \gamma\pi + (\epsilon - \gamma) \int_0^{\pi} G(x, \delta, \tau)\, dx \qquad (16)$$

The values of x_i are computed numerically by first evaluating $X'(x)'$ and then $X(x)$ on a very fine working grid in x.

With this definition of the half-width δ, the stretching at $x_0 \pm \delta$ is $(\gamma + \epsilon)/2 \simeq \gamma/2$ (ϵ is smaller than 1 and γ generally much greater than 1), so that the grid is already twice coarser here than in the zoom center. For x such that

$$\frac{\tau(\delta - |x|)}{|x|(\pi - |x|)} = 1 \qquad (17)$$

(so that $G = (1 - \tanh 1)/2 \simeq 0.12$), the stretching factor is $g = 0.88\gamma + 0.12\epsilon \simeq 0.88\gamma$. This leads to a possible definition for an effective half-width δ_{eff} related to δ by $\delta_{\text{eff}} = \delta - \frac{\delta_{\text{eff}}}{\tau}(\pi - \delta_{\text{eff}})$. For $x = x_0 \pm \delta_{\text{eff}}$, the grid is only about 10% coarser than at the zoom center. For a given value of the effective width, the difference $\delta - \delta_{\text{eff}}$ decreases as the inverse of the stiffness coefficient τ.

The approach is similar for latitudes. The zoomed latitudes, y, are defined with respect to regular latitudes, Y, by specifying a stretching factor, $g(y)$, defined for y in $[y_0 - \Delta, y_0 + \Delta]$, with $\Delta = |y_0| + \pi/2$, on a symmetric domain with respect to the zoom center y_0, going from the pole of the hemisphere opposite to the zoom center and extending virtually beyond the pole in the hemisphere of the zoom. The stretching factor is given by

$$Y'(y) = g(y) = \gamma + (\epsilon - \gamma) G(y - y_0, \delta, \tau) \qquad (18)$$

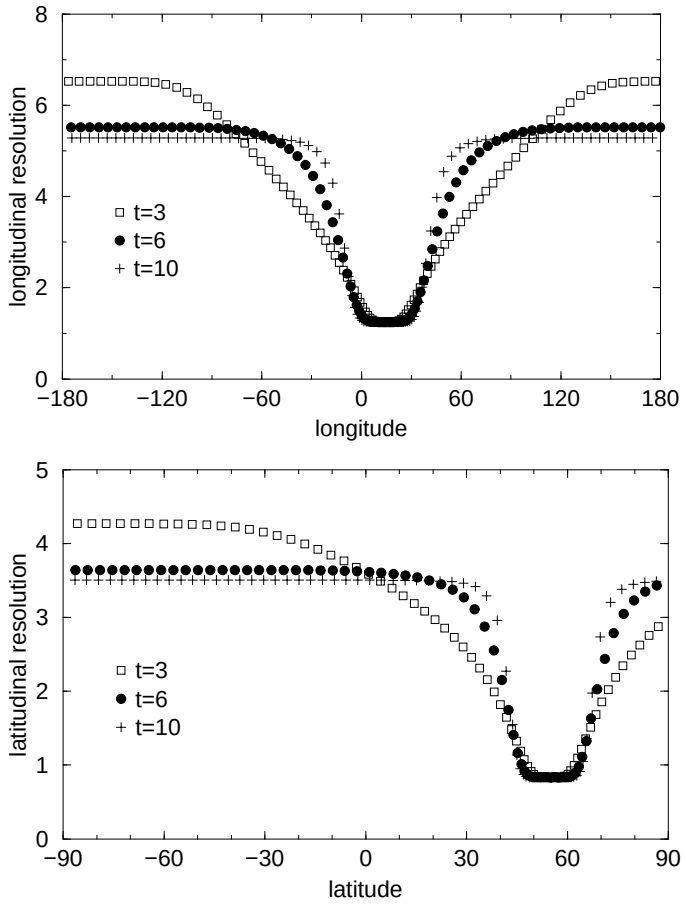

FIG. 17: Longitudinal and latitudinal resolution (in degrees) of the LMDZ grid with x_0 =15E, y_0=55N, $\delta_x = 43.2^o$, $\delta_y = 21.6^o$ and $\gamma = 3$ for both directions. The resolution is shown both for the grid used for the ETEX simulations presented above, with $\tau = 6$ in both directions, as well as for $\tau = 3$ and $\tau = 10$.

with

$$G(y, \delta, \tau) = \frac{1}{2}\left\{1 - \tanh\left[\frac{\tau(\delta - |y|)}{|y|(\Delta - |y|)}\right]\right\} \qquad (19)$$

The condition to be imposed is that y varies from $-\pi/2$ to $\pi/2$ when Y varies from $-\pi/2$ to $\pi/2$ so that ϵ is given by

$$\pi = \pi\gamma + (\epsilon - \gamma)\int_{-\pi/2}^{\pi/2} G(y - y_0, \delta, \tau)\, dy \qquad (20)$$

For the control simulation presented above, the center of the zoom, (x_0, y_0), is fixed at (15E,55N) and the width δ in x and y at 43.2^o and 21.6^o respectively. In both directions we use a zoom factor of 3 and a stiffness coefficient of 6 in both directions. Fig. 17 shows the longitudinal and latitudinal resolutions for this grid as well as examples with different stiffness coefficients.

References

Boucher, O. and Pham, M. (2002). History of sulfate aerosol radiative forcings. *Geophys. Res. Lett.*, 29:22–1.

Cressman, G. P. (1959). An operational objective analysis system. *Mon. Wea. Rev.*, 87:367–374.

Dufresne, J.-L., Quaas, J., Boucher, O., Denvil, S., and Fairhead, L. (2005). Contrasts in the effects on climate of anthropogenic sulfate aerosols between the XXth and XXIst centuries. Geophys. Res. Lett., in press.

Forget, F., Hourdin, F., Fournier, R., Hourdin, C., Talagrand, O., Collins, M., Lewis, S. R., Read, P. L., and Huot., J.-P. (1999). Improved general circulation models of the Martian atmosphere from the surface to above 80 km. *J. Geophys. Res.*, 104:24,155–24,176.

Fouquart, Y. and Bonnel, B. (1980). Computations of solar heating of the Earth's atmosphere: A new parametrization. *Contrib. Atmos. Phys.*, 53:35–62.

Godunov, S. K. (1959). Finite-difference methods for the numerical computations of equations of gas dynamics. *Math. Sb.*, 7:271–290.

Graziani, C., Klug, W., and Mosca, S. (1996). Real-time long-range dispersion model evaluation of the ETEX release. Technical report, Joint Research Center, Office for Official Publications of the European Communities.

Hauglustaine, D. A., Hourdin, F., Jourdain, L., Filiberti, M.-A., Walters, S., Lamarque, J.-F., and Holland, E. A. (2004). Interactive chemistry in the Laboratoire de Météorologie Dynamique general circulation model: Description and background tropospheric chemistry evaluation. *J. Geophys. Res.*, 109:4314–4357.

Hourdin, F. and Armengaud, A. (1999). Test of a hierarchy of finite-volume schemes for transport of trace species in an atmospheric general circulation model. *Mon. Wea. Rev.*, 127:822–837.

Hourdin, F., Idelkadi, A., and Talagrand, O. (2005). Eulerian backtracking of atmospheric tracers: II numerical aspects. QJRMS, in press.

Hourdin, F. and Issartel, J.-P. (2000). Sub-surface nuclear tests monitoring through the CTBT xenon network. *Geophys. Res. Lett.*, 27:2245–2248.

Hourdin, F., Le Van, P., Forget, F., and Talagrand, O. (1993). Meteorological variability and the annual surface pressure cycle on Mars. *J. Atmos. Sci.*, 50:3625–3640.

Hourdin, F., Lebonnois, S., Luz, D., and Rannou, P. (2004). Titan's stratospheric composition driven by condensation and dynamics. *J. Geophys. Res.*, pages 12005–+.

Hourdin, F. and Talagrand, O. (2005). Eulerian backtracking of atmospheric tracers: I adjoint derivation and parametrization of subgrid-scale transport. QJRMS, in press.

Hourdin, F., Talagrand, O., Sadourny, R., Régis, C., Gautier, D., and McKay, C. P. (1995). General circulation of the atmosphere of Titan. *Icarus*, 117:358–374.

Idelkadi, A. (2002). *Validation du transport atmosphérique direct et inverse des espèces traces aux échelles continentales dans un modèle de circulation générale atmosphérique à grille variable.* thèse, Université Paris-6.

Jeuken, A. B. M., Siegmund, P. C., C., H. L., Feichter, J., and Bengtsson, L. (1996). On the potential of assimilating meteorological analyses in a global climate model for the purpose of model validation. *J. Geophys. Res.*, 101:939.

Kasahara, A. (1977). Computational aspects of numerical models for weather prediction and climate simulation. In Chang, J., editor, *Methods in computational physics*, volume 17, pages 1–66. Academic press, inc.

Klug, W., Graziani, G., Grippa, G., Pierce, D., and Tassone, C. (1992). Evaluation of long range atmospheric transport models using environmental radioactivity data from the chernobyl accident. *Elsevier Sciences Publishers*, pages 18–28.

Krinner, G., Genthon, C., Li, Z., and Le Van, P. (1997). Studies of the Antarctic climate with a stretched-grid general circulation model. *J. Geophys. Res.*, 102:13731–13746.

Laval, K., Sadourny, R., and Serafini, Y. (1981). Land surface processes in a simplified general circulation model. *Geophys. Astrophys. Fluid Dyn.*, 17:129–150.

Le Treut, H., Li, Z., and Forichon, M. (1994). Sensitivity study of the LMD GCM to greenhouse forcing associated with two different cloud water parametrizations. *J. Clim*, 7:1827–1841.

Le Treut, H. and Li, Z. X. (1991). Sensitivity of an atmospheric general circulation model to prescribed SST changes: Feedback effects associated with the simulation of cloud optical properties. *Climate Dynamics*, 5:175–187.

Lefèvre, F., Lebonnois, S., Montmessin, F., and Forget, F. (2004). Three-dimensional modeling of ozone on Mars. *J. Geophys. Res. (planets)*, 109(E18):7004–+.

Li, Z. (1999). Ensemble Atmospheric GCM Simulation of Climate Interannual Variability from 1979 to 1994. *Journal of Climate*, 12:986–1001.

Li, Z. X. and Conil, S. (2003). A 1000-year simulation with the IPSL ocean-atmosphere coupled model. *Annals of Geophysics*, 46(1):39–46.

Lin, S.-J. and Rood, R. B. (1996). Multi-dimensional flux form semi-lagrangian transport schemes. *Mon. Wea. Rev.*, 124:2046–2070.

Louis, J.-F. (1979). A parametric model of vertical eddy fluxes in the atmosphere. *Boundary-layer Meteorol.*, 17:187–202.

Marti, O., Braconnot, P., Bellier, J., Benshila, R., Bony, S., Brockmann, P., Cadule, P., Caubel, A., Denvil, S., Dufresne, J.-L., Fairhead, L., Filiberti, M.-A., Foujols, M.-A., Fichefet, T., Friedlingstein, P., Grandpeix, J.-Y., Hourdin, F., Krinner, G., Lévy, C., Madec, G., Musat, I., de Nolbet, N., Polcher, J., and Talandier, C. (2005). The new IPSL climate system model: IPSL-CM4. Technical note, IPSL. available at http://dods.ipsl.jussieu.fr/omamce/IPSLCM4/DocIPSLCM

Mickley, L. J., Murti, P. P., Jacob, D. J., Logan, J. A., Koch, D. M., and Rind, D. (1999). Radiative forcing from tropospheric ozone calculated with a unified chemistry-climate model. *J. Geophys. Res.*, 104:30153–30172.

Morcrette, J. J., Smith, L., and Fouquart, Y. (1986). Pressure and temperature dependence of the absorption in longwave radiation parametrizations. *Contrib. Atmos. Phys.*, 59(4):455–469.

Pasquill, F. and Smith, F. (1983). Atmospheric diffusion, 3d ed. *Wiley and Sons.*

Prather, M. J. (1986). Numerical advection by conservation of second order moments. *J. Geophys. Res.*, 91:6671–6681.

Rannou, P., Hourdin, F., and McKay, C. P. (2002). A wind origin for Titan's haze structure. *Nature*, 418:853–856.

Robert, A. (1981). A stable numerical integration scheme for the primitive meteorological equations. *Atmos. Ocean*, 19:35–46.

Rood, R. B. (1987). Numerical advection algorithms and their role in atmospheric transport and chemistry models. *Rev. Geophys.*, 25:71–100.

Sadourny, R. and Laval, K. (1984). January and July performance of the LMD general circulation model. In Berger, A. and Nicolis, C., editors, *New perspectives in Climate Modeling*, Elsevier, pages 173–197. Amsterdam.

Shindell, D. T., Lee Grenfell, J., Rind, D., Grewe, V., and Price, C. (2001). Chemistry-climate interactions in the Goddard Institute for Space Studies general circulation model, 1, Tropospheric chemistry model description and evaluation. *J. Geophys. Res.*, pages 8047–8076.

Simmons, A. J. and Burridge, D. M. (1981). An energy and angular momentum conserving verical finite-difference scheme and hybrid vertical coordinates. *Mon. Wea. Rev.*, 109:758–766.

Staniforth, A. and Côté, C. (1991). Semi-lagrangian integration schemes for atmospheric models. *Mon. Weather Rev.*, 119:2206.

Taylor, J., Brasseur, P., Zimmerman, P., and Cicerone, R. (1991). A study of the sources and sinks of methane and methyl chloroform using a global three-dimensional lagrangian tropospheric tracer transport model. *J. Geophys. Res.*, 96:3013.

Tiedtke, M. (1989). A comprehensive mass flux scheme for cumulus parameterization in large-scale models. *Mon. Wea. Rev.*, 117:1179–1800.

Van Dop, H. and Nodop, K., editors (1998). *ETEX, A european tracer experiment*, volume 32 of *Atmos. Environn. special issue, pp. 4089–4378.*

Van Leer, B. (1977). Towards the ultimate conservative difference scheme : IV. a new approach to numerical convection. *J. Computational Phys.*, 23:276–299.

Walton, J., MacCracken, M., and Ghan, S. (1988). A global-scale lagrangian trace species model of transport, transformation and removal process. *J. Geophys. Res.*, 93:8339.

Williamson, D. and Rasch, P. J. (1989). Two dimensional semi-lagrangian transport with shape-preserving interpolation. *Mon. Wea. Rev.*, 117:102–127.

Yabe, T., Tanaka, R., Nakamura, T., and Xiao, F. (2001). An exactly conservative semi lagrangian scheme (CIP-CSL) in one dimension. *Mon. Wea. Rev.*, 129:332–344.